Crystal Structure of Cobalt-Substituted Calcium Hydroxyapatite Nanopowders Prepared by Hydrothermal Processing

Article *in* Journal of Applied Crystallography · April 2010

DOI: 10.1107/S0021889809051395/ks5226sup2.rtv

CITATIONS
22

READS
765

8 authors, including:

Zoran Slobodan Stojanovic
Serbian Academy of Sciences and Arts
30 PUBLICATIONS **712** CITATIONS
SEE PROFILE

Ines Bracko
Novartis
19 PUBLICATIONS **562** CITATIONS
SEE PROFILE

Smilja Markovic
Serbian Academy of Sciences and Arts
123 PUBLICATIONS **1,778** CITATIONS
SEE PROFILE

Nenad L. Ignjatovic
Serbian Academy of Sciences and Arts
165 PUBLICATIONS **2,767** CITATIONS
SEE PROFILE

Journal of
Applied Crystallography
ISSN 0021-8898
Editor: **Anke R. Pyzalla**

Crystal structure of cobalt-substituted calcium hydroxyapatite nanopowders prepared by hydrothermal processing

Ljiljana Veselinović, Ljiljana Karanović, Zoran Stojanović, Ines Bračko, Smilja Marković, Nenad Ignjatović and Dragan Uskoković

J. Appl. Cryst. (2010). **43**, 320–327

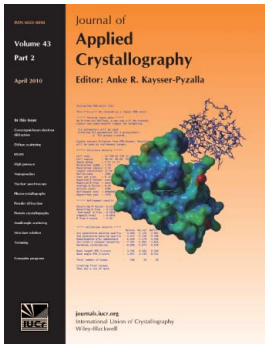

Journal of
Applied Crystallography
ISSN 0021-8898

Received 27 April 2009
Accepted 28 November 2009

Crystal structure of cobalt-substituted calcium hydroxyapatite nanopowders prepared by hydrothermal processing

Ljiljana Veselinović,[a] Ljiljana Karanović,[b] Zoran Stojanović,[a] Ines Bračko,[c] Smilja Marković,[a] Nenad Ignjatović[a] and Dragan Uskoković[a]*

[a]Institute of Technical Sciences of the Serbian Academy of Sciences and Arts, Knez Mihailova 35/IV, 11001 Belgrade, Serbia, [b]Laboratory for Crystallography, Faculty of Mining and Geology, University of Belgrade, Đušina 7, 11000 Belgrade, Serbia, and [c]Jožef Stefan Institute, Jamova 39, 1000 Ljubljana, Slovenia. Correspondence e-mail: dragan.uskokovic@itn.sanu.ac.rs

A series of cobalt-exchanged hydroxyapatite (CoHAp) powders with different Ca/Co ratios and nominal unit-cell contents $Ca_{10-x}Co_x(PO_4)_6(OH)_2$, x = 0, 0.5, 1.0, 1.5 and 2.0, were synthesized by hydrothermal treatment of a precipitate at 473 K for 8 h. Based on ICP (inductively coupled plasma) emission spectroscopy analysis, it was established that the maximum amount of cobalt incorporation saturated at ~12 at.% under these conditions. The effects of cobalt content on the CoHAp powders were investigated using ICP emission spectroscopy, particle size analysis, transmission electron microscopy (TEM) and high-resolution transmission electron microscopy (HRTEM) analyses as well as X-ray powder diffraction (XRPD) including Rietveld analysis. According to XRPD, all the materials are single-phase HAp and CoHAp of low crystallinity. Rietveld analysis shows that Co enrichment causes the c cell parameter to decrease at a faster rate than the a cell parameter. A microstructural analysis showed anisotropic X-ray line broadening due to crystallite size reduction. In CoHAp there is significant crystal elongation in [001], and the average size decreases with increasing cobalt content. The crystallite morphology transforms from rod-like for the pure HAp to lamellae at the highest degree of Co substitution. The results of Rietveld refinement (symmetry, size and morphology of the crystallites) were confirmed by TEM and HRTEM analysis.

1. Introduction

In the 1960s, the hexagonal structure of hydroxyapatite which possesses hydroxyl ions in twofold disorder [HAp, $Ca_{10}(PO_4)_6(OH)_2$] was determined by Kay *et al.* (1964), Sudarsanan & Young (1969) and Posner *et al.* (1958). Monoclinic hydroxyapatite with ordered anion (hydroxyl) columns also exists, and was described by Elliott *et al.* (1973) and Suetsugu & Tanaka (2002). Over the following years, many researchers studied the structure of hydroxyapatite, from different aspects, because of its wide applicability in medicine, ecology and catalysis (Jevtić *et al.*, 2008; Pan & Darvell, 2009; Suvorova & Buffat, 2001). HAp mostly crystallizes in $P6_3/m$, with two formula units $[Ca_5(PO_4)_3(OH)]$ per unit cell (Elliott, 1994; Mostafa & Brown, 2007; Stork *et al.*, 2005).

The unit cell $M1_4M2_6(PO_4)_6(OH)_2$ of HAp exhibits two crystallographically independent cationic sites, $M1$ and $M2$. The $M1$ cations, which are located at the 4*f* Wyckoff position, are bonded to nine O atoms of the PO_4 tetrahedra, while the $M2$ cations at the 6*h* Wyckoff position are coordinated by six O atoms of the PO_4 tetrahedra and by one of the OH^- ions positioned in the channel running along the [001] direction. Ca ions at the $M1$ site are aligned in columns of tricapped metaprisms which share trigonal basal planes (Fig. 1*a*), while calcium ions at the $M2$ site build equilateral triangles centred

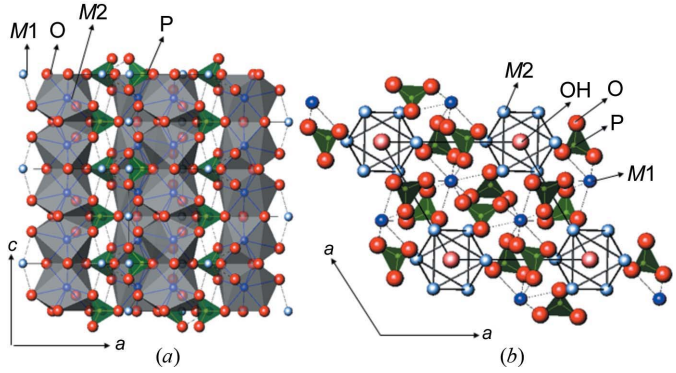

Figure 1
(*a*) The chains of the $M1O_9$ polyhedra in HAp running parallel to the c axis with neighbouring PO_4 coordination tetrahedra as viewed along [010]. (*b*) The crystal structure of HAp viewed along [001]. The largest dark spheres represent $M1$ sites. $M2$ positions are connected in triangles around the anion, *i.e.* OH^- group in the channel. PO_4 coordination tetrahedra are shaded.

on the 6_3 screw axes (Fig. 1*b*) (White & ZhiLi, 2003; Kannan *et al.*, 2008; Ma & Ellis, 2008; De Leeuw, 2001; Badraoui *et al.*, 2007). Neighbouring *M*1- and *M*2-centred polyhedra are linked through O atoms of the PO_4 tetrahedra.

Because of the high stability and flexibility of the hydroxyapatite structure, a great number of substitutions, both cationic and anionic, are possible. Calcium ions can be replaced by various divalent cations including Sr^{2+}, Ba^{2+}, Pb^{2+}, Zn^{2+}, Cd^{2+} and Co^{2+} (Stojanović *et al.*, 2009; Shi *et al.*, 2006; Elkabouss *et al.*, 2004; Riberio *et al.*, 2006; Li *et al.*, 2008; Ergun, 2008; Wang *et al.*, 2008; Anmin *et al.*, 2007; Đordević *et al.*, 2008; Yuanzhi *et al.*, 2009). For these systems the miscibility limit can be correlated to the relative ionic properties (polarizability, electronegativity and cationic size; Brückner *et al.*, 1995; Bigi *et al.*, 1989; Badraoui *et al.*, 2001). Cations such as Sr^{2+}, Ba^{2+} and Pb^{2+}, which are larger than Ca^{2+}, show a strong preference for the larger *M*2 site, while smaller ions usually occupy the *M*1 site (Zhu *et al.*, 2006). Moreover, electronegativity has a great influence on the distribution of the cations between the two sites. Cations with higher electronegativity demonstrate a great affinity for covalent interactions, and for bonding with hydroxyl groups (Pearson, 1988; Wu *et al.*, 2007; Low *et al.*, 2008). The different substituents have a great influence on HAp properties, particularly the unit-cell parameters, the degree of crystallinity, crystallite size and morphology.

Partial replacement of calcium ions in HAp with magnetic metal ions (Fe, Co, Ni *etc.*) without collapse of the crystal structure can lead to magnetic ordering. Recently, Wu *et al.* (2007) reported novel biomagnetic nanoparticle composites based on hydroxyapatite which possess superparamagnetic properties and good biocompatibility, and which may find application in magnetic cell separation, cell labelling for high-resolution magnetic resonance imaging, targeted drug and/or gene delivery, and hyperthermia treatment (Pankhurst *et al.*, 2003; Dodd *et al.*, 1999; Jain *et al.*, 2008).

This paper reports the hydrothermal synthesis of new apatites having the general formula $(Ca,Co)_{10}(PO_4)_6(OH)_2$. The compounds were characterized chemically, morphologically and structurally. The main goal of this study was to define the influence of partial replacement of calcium by cobalt on the crystal structure, particle and crystallite morphology, and crystallite size.

2. Experimental

2.1. Materials preparation

HAp and cobalt-substituted hydroxyapatite (CoHAp) powders were prepared by hydrothermal treatment of precipitates. Firstly, HAp powders were prepared at different temperatures in order to find the optimal conditions for the preparation of pure hydroxyapatite without impurities and/or second phase(s). The HAp precipitate was prepared by adding a filtered supersaturated alkaline solution of $Ca(NO_3)_2$ dropwise into a mixture of H_3PO_4 and ammonia water at 323 K, under constant stirring (700 r min^{-1}). Then, suspensions were hydrothermally treated in a 2 l Parr stainless steel stirred reactor under non-equilibrium conditions up to 523 K at a constant heating rate of 2 K min^{-1} and fixed stirring rate (400 r min^{-1}). Samples were taken from the autoclave at 373, 423, 473 and 523 K. In our previous paper (Stojanović *et al.*, 2009) we presented the results of a detailed examination of the HAp powders, where it was shown that temperatures over 473 K caused a partial transition of HAp to β-tricalcium phosphate (β-TCP). Therefore, hydrothermal treatment at 473 K was chosen for the synthesis of CoHAp powders. The reagents were adjusted to obtain CoHAp with nominal unit-cell contents $Ca_{10-x}Co_x(PO_4)_6(OH)_2$, $x = 0$, 0.5, 1.0, 1.5 and 2.0 (respectively, referred to as HAp, Co5HAp, Co10HAp, Co15HAp and Co20HAp). A supersaturated alkaline solution of $Ca(NO_3)_2$ and an aqueous solution of $Co(NO_3)_2$ were simultaneously added dropwise to a mixture of H_3PO_4 and ammonia water under the same conditions, with the ratio of (Ca + Co)/P fixed at 1.67. Each suspension (about 1 l in volume) was then treated in the autoclave at 473 K for 8 h and an autogenous pressure of 2 MPa, under constant stirring (400 r min^{-1}). After treatment, the autoclave was quenched to room temperature. The precipitate was washed with distilled water to remove NH_4^+ ions and potentially adsorbed Co^{2+} ions, and then dried at 363 K in air for 24 h.

It should be emphasized that, during the precursor preparation procedure, we used degassed water and barbotated Ar through the solution, in order to minimize the effect of oxidation of the cobaltous ammonia complex to the cobaltic one. After the precipitation had been completed, the colour of the mother liquor was rose, whereas the precipitate was dark rose. Therefore, we supposed that the greatest part of the cobalt ions present in our system were in the 2+ oxidation state; this was further confirmed by magnetic measurement.

2.2. Materials characterization

The chemical analysis was carried out using an inductively coupled plasma (ICP) spectrometer (iCAP Thermo Scientific 6300). Before the analysis, all samples were diluted in concentrated HCl.

The average particle size and particle size distribution were determined by a particle size analyser (PSA) based on laser diffraction with a Mastersizer 2000 (Malvern Instruments Ltd, UK), which covers the range 0.02–2000 µm. For the PSA measurements the powders were ultrasonically dispersed (low-intensity ultrasound, at a frequency of 40 kHz and power of 50 W) for 3 min in distilled water.

X-ray powder diffraction (XRPD) analysis[1] was used to identify the crystal phases in the synthesized powders and for the Rietveld refinement. The XRPD data were recorded on a Philips PW 1050 diffractometer with Cu $K\alpha_{1,2}$ ($\lambda = 1.54178$ Å) Ni-filtered radiation. The diffraction intensity was measured from 8 to 110° 2θ, using a step size of 0.02° with a counting time of 12 s $step^{-1}$. The working conditions were 40 kV and

[1] Supplementary material for this paper is available from the IUCr electronic archives (Reference: KS5226). Services for accessing these data are described at the back of the journal.

Table 1
The notation, nominal composition and unit-cell contents obtained by both ICP and Rietveld analysis.

Notation	Nominal composition	ICP analysis	Rietveld analysis
HAp	$Ca_{10}(PO_4)_6(OH)_2$	$Ca_{10}(PO_4)_6(OH)_2$	$Ca_{10}(PO_4)_6(OH)_2$
Co5HAp	$Ca_{9.5}Co_{0.5}(PO_4)_6(OH)_2$	$Ca_{9.57}Co_{0.43}(PO_4)_6(OH)_2$	$Ca_{9.74}Co_{0.26}(PO_4)_6(OH)_2$
Co10HAp	$Ca_9Co(PO_4)_6(OH)_2$	$Ca_{9.05}Co_{0.95}(PO_4)_6(OH)_2$	$Ca_{9.27}Co_{0.73}(PO_4)_6(OH)_2$
Co15HAp	$Ca_{8.5}Co_{1.5}(PO_4)_6(OH)_2$	$Ca_{8.85}Co_{1.17}(PO_4)_6(OH)_2$	$Ca_{9.26}Co_{0.74}(PO_4)_6(OH)_2$
Co20HAp	$Ca_8Co_2(PO_4)_6(OH)_2$	$Ca_{8.85}Co_{1.15}(PO_4)_6(OH)_2$	$Ca_{9.19}Co_{0.81}(PO_4)_6(OH)_2$

20 mA. The Rietveld refinements were performed using *FullProf* in the *WinPLOTR* environment (McCusker *et al.*, 1999; Young, 1993; Rodriguez-Carvajal, 1990, 2005; Roisnel & Rodrigez-Carvajal, 2001). The unit-cell parameters were calculated using the program *LSUCRI* (Garvey, 1986). The Rietveld refinements started from the fixed unit-cell parameters calculated by *LSUCRI* and atomic positions reported previously (Rodriguez-Lorenzo *et al.*, 2003). The peak profiles were described by a Thompson–Cox–Hastings (TCH) pseudo-Voigt profile function, whereas linear interpolation between selected points was used for the background description.

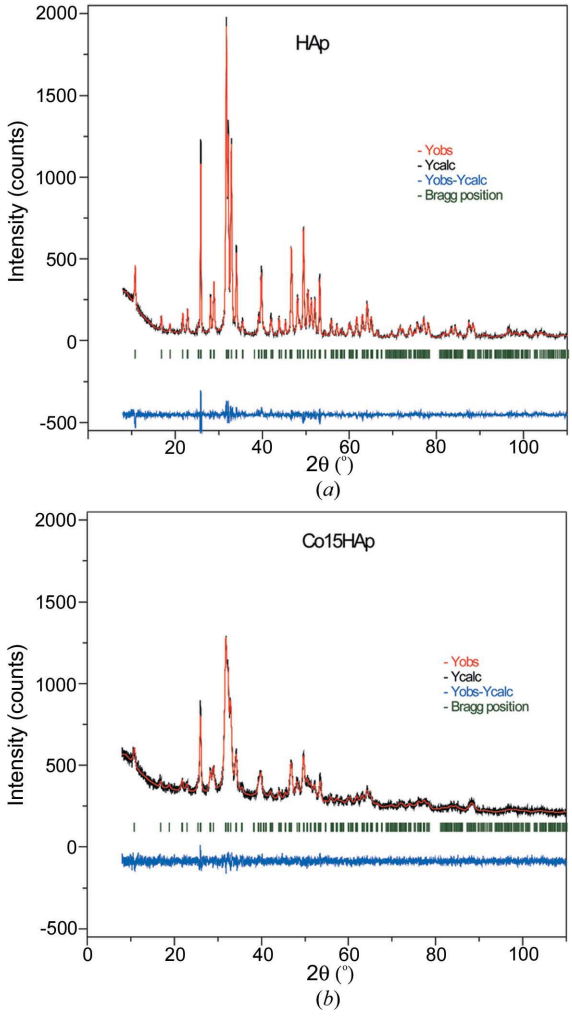

Figure 2
Final Rietveld refined plots of (*a*) HAp and (*b*) Co15HAp.

Scattering factors for the neutral atoms were applied for the refinements. After refinement, the individual isotropic atomic displacement parameters were too large and were fixed at 1.5 Å^2. Finally, the occupation numbers were allowed to vary in both *M*1 and *M*2 sites, keeping the isotropic atomic displacement parameters at fixed values. The occupancy factors of O and P were not refined, in agreement with HAp stoichiometry. Additionally, in order to keep the geometry of the PO_4 tetrahedron reasonable, a geometric restraint on the P—O bond distances of 1.53 (2) Å was used.

From reflection broadening, the average crystallite size was estimated through the refinement of the TCH pseudo-Voigt function parameters and multipolar functions (Antić *et al.*, 2004; Cvejic *et al.*, 2006; Stephens, 1999). In order to exclude instrumental broadening, the XRPD pattern of a CeO_2 standard was fitted (U = 0.027100, V = −0.010800, W = 0.020700, X = 0.008000, Y = 0.025706).

The microstructure and morphology of the synthesized powders were investigated by transmission electron microscopy (TEM) (using a Jeol 2100, operating at 200 kV). The powders for TEM observation were dispersed in acetone ultrasonically and deposited on holey carbon films supported by a 300-mesh copper grid.

Fourier transform–infrared spectroscopy (FT–IR) measurements were performed on a MIDAC M 2000 Series Research Laboratory FT–IR spectrometer using the KBr pellet technique, in the spectral range of 400–4000 cm^{-1}. The spectral resolution was 4 cm^{-1}.

Magnetic measurement was carried out in the high-temperature (*i.e.* paramagnetic) region 100 < T < 300 K using Quantum Design's superconducting quantum interference device-based magnetometer MPMS XL-5.

3. Results and discussion

In our previous paper (Stojanović *et al.*, 2009) we presented the preliminary characterization of hydrothermally prepared microcrystalline samples of CoHAp. Here we report the results of a structural data analysis of CoHAp powders with respect to some geometric characteristics, such as unit-cell parameters, ionic radii and bond distances. In addition, the chemical composition, average particle size, particle size distribution and morphology of agglomerates with respect to the cobalt content in the CoHAp crystal structure are reported.

The amounts (in wt%) of Ca and Co in the powders were determined by ICP emission spectroscopy analysis, with an error of ± 1 and ± 0.1%, respectively. The number of Ca and Co atoms (in at.%, in relation to 10 atoms of Ca + Co in CoHAp) in the unit cell of CoHAp was calculated and stoichiometric formulae are listed in Table 1. ICP analysis showed that the total content of Co ions incorporated in CoHAp was 4.3, 9.5, 11.7 and 11.5 at.%, respectively, for the samples Co5HAp, Co10HAp, Co15HAp and Co20HAp. Under these hydrothermal processing conditions, the maximum cobalt

Table 2
Unit-cell parameters, cell volume and metaprism twist angle φ for $Ca_{10-x}Co_x(PO_4)_6(OH)_2$, x = 0, 0.5, 1.0, 1.5 and 2.0.

Sample	a (Å)	c (Å)	V (Å^3)	φ (°)
Hughes *et al.* (1989)	9.4166†	6.8745†	527.91†	23.1
Mostafa & Brown (2007)	9.412†	6.853†	525.75†	24.8
Stork *et al.* (2005)	9.438†	6.887†	531.28†	23.5
HAp	9.4210 (1)	6.8800 (1)	528.83 (1)	23.8
Co5HAp	9.4170 (3)	6.8671 (2)	527.38 (3)	23.6
Co10HAp	9.4039 (2)	6.8525 (6)	524.81 (4)	23.4
Co15HAp	9.4109 (5)	6.8455 (5)	525.05 (5)	22.3
Co20Hap	9.4072 (3)	6.8399 (2)	524.21 (5)	22.5

† Standard uncertainty values were not stated in the articles.

incorporated saturated at 11.7 at.%, and further increases in cobalt reagent concentration did not enhance Co^{2+} content in the crystal structure.

The particle size distribution (based on number) of pure HAp powder, prepared by the hydrothermal method at 473 K, was very narrow (span = 1.075), with an average particle size of 94 nm. The incorporation of 4.3 at.% Co^{2+} in the Ca^{2+} positions provoked a reduction in average particle size to 63 nm, and a broadening of the particle size distribution (span = 1.338). Further increases in the cobalt content, up to 9.5 at.%, did not change either the average particle size or the particle size distribution. The average particle size was 64 nm, whereas the span was 1.387. Furthermore, the incorporation of about 12 at.% Co^{2+} into HAp yielded a powder with particles of average size 71 nm and a narrow particle size distribution with a span of 1.356.

The agreement between the observed and calculated powder patterns refined using the Rietveld method for pure HAp and the sample with the highest degree of substitution (Co15HAp) is illustrated in Fig. 2. All of the powders were refined as single-phase HAp and CoHAp, irrespective of cobalt content in the powders. The refined unit-cell parameters and cell volumes are given in Table 2.

The unit-cell parameters of the prepared HAp mostly agree, within ±0.002 Å, with literature values (Table 2). The unit-cell parameters of the CoHAp phases mainly depend on cobalt content (Denton & Ashcroft, 1990; Kuo *et al.*, 2004). With the increase in cobalt content, the reflections were shifted to higher 2θ angles as a result of decreasing unit-cell parameters due to the incorporation of smaller Co^{2+} at *M*1 and *M*2. The relationship between the unit-cell parameters of HAp and CoHAp phases *versus* the Co content shows a faster change in the c than in the a dimension (Fig. 3).

While studying the crystal structure of the cobalt-substituted HAp, we examined the possibility that Co^{2+} cations are located in the calcium positions and/or in the tunnels (by replacing OH^-). It is known from the literature that the replacement of Ca by ions with smaller ionic radius provokes a decrease in cell volume (Zhu *et al.*, 2006; White & ZhiLi, 2003; Low *et al.*, 2008). In addition, Baikie *et al.* (2009) and Kazin *et al.* (2007) demonstrated that the incorporation of 3d-metal ions (Ni^{2+}, Co^{2+}, Zn^{2+}, Cu^{2+}) in the hexagonal channel of the apatite structure causes the expansion of the unit cell. Our results, obtained by Rietveld refinement, show a decrease in cell volume with increasing cobalt content in the structure, indicating the incorporation of cobaltous ions in the calcium positions. This statement is in accordance with the results of vibrational (Raman and FT–IR) spectroscopy analysis of CoHAp samples.

In our previous paper (Stojanović *et al.*, 2009) Raman spectra of CoHAp samples were analysed. Comparing the spectra of the CoHAp samples with that of pure HAp, it is seen that the Raman bands of the CoHAps coincide with those of HAp. The overall spectrum does not change in terms of the band number and position. A considerable line broadening and a decrease in the intensity ratio from HAp to Co20HAp are attributed to the incorporation of smaller Co^{2+} in the Ca^{2+} crystallographic positions in the HAp structure.

In addition, we investigated FT–IR spectra of the CoHAp samples. The FT–IR spectrum of pure HAp has typical apatite phosphate (PO_4^{3-}) modes near 565, 603, 962, 1035 and 1095 cm^{-1}; that of the water associated with HAp at 3440 cm^{-1}; and that of OH^- libration and stretching modes at 635 and 3570 cm^{-1}, respectively. We found that the vibrational

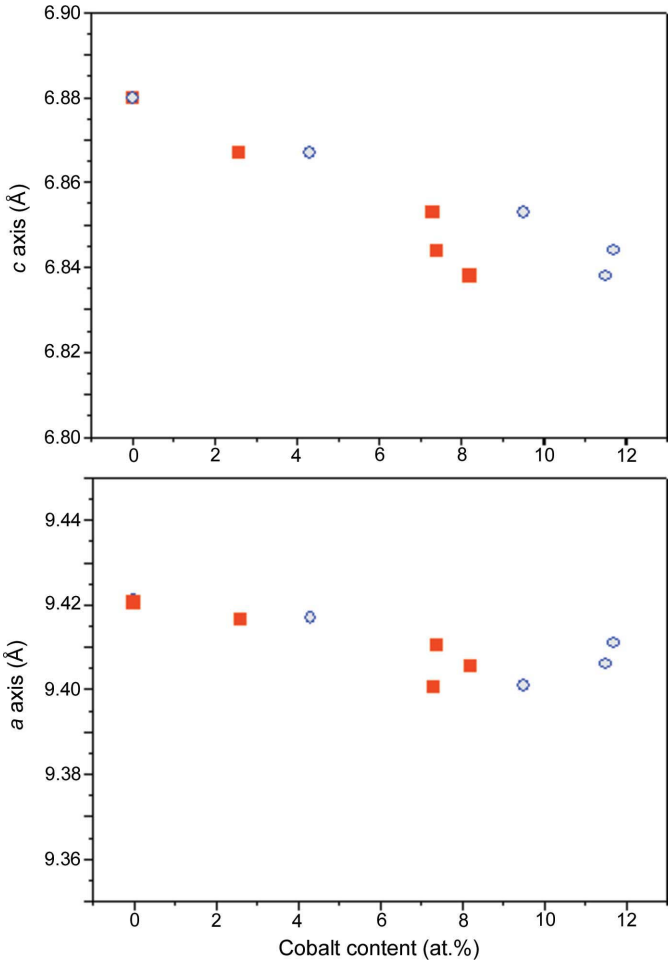

Figure 3
Relationship between the unit-cell parameters and the cobalt content in HAp and CoHAp phases. Blue circles correspond to the values of cobalt content obtained by ICP analysis; red squares demonstrate cobalt content obtained based on occupancy factors.

bands of the CoHAp samples coincide with those of HAp. Because the Co—O bond length is shorter than that of Ca—O and the O—H bond was weakened, the intensity of the stretching vibration band of OH^- decreased with the increase in cobaltous content incorporated in the crystallographic positions of calcium.

Kazin *et al.* (2007), who dealt with the distribution of 3d-metal ions in the channels, observed some peculiarities in the IR spectra. They observed two weak bands in the region of the OH^- stretching vibrations. One is assigned to the OH groups disturbed by the presence of 3d-metal ions in the channels (when the O—H···O—*M*—O···H—O fragments are formed), while the second is assigned to the undisturbed OH groups.

The lack of the stretching band attributed to the OH groups disturbed by the presence of 3d-metal ions in the channels in the FT–IR spectra of CoHAp is yet further proof that Co^{2+} ions are incorporated into the Ca^{2+} crystallographic positions.

Thus, crystallographic and vibrational–spectroscopic evidence suggests that cobaltous ions are distributed over the Ca^{2+} crystallographic positions.

The refined atomic positions and occupancy factors are presented in Table 3.

As the amount of Co^{2+} increased, the diffraction intensity notably decreased and broadened, indicating lower crystallinity. Microstructural analysis shows a decrease in the crystallite size and changes in morphology with cobalt content. The mean values of crystallite size decrease from 58 to 23, 21, 20 and 18 nm for HAp, Co5HAp, Co10HAp, Co15HAp and Co20HAp, respectively (Fig. 4), and are somewhat smaller than the average dimensions observed by particle size analysis (94, 63, 64, 70 and 71 nm). The discrepancy is due to the presence of aggregates in the particle-size-analysed powders. The structure refinement indicated X-ray line broadening anisotropy as a consequence of the anisotropic growth of crystallites. Anisotropy is changed according to variation of ionic radius of the exchanged ions (Stephens, 1999; Jeanjean *et al.*, 1994; Järvinen, 1993). The incorporation of cobalt ions in the HAp structure causes a decrease in both anisotropy and crystallite size. Based on the studied values of crystallite size along different [*hkl*] directions, significant elongation occurs along the *c* axis, leading to rod-like morphology; the elongation decreased with increasing cobalt content leading to the formation of lamellae (Fig. 5). Similar phenomena were also observed by Stephens (1999), Cvejic *et al.* (2006) and Vallet-Regi & Arcos (2005).

Table 4 summarizes the metal–oxygen bond distances for pure and cobalt-substituted HAp samples. In addition, the incorporation of Co^{2+} causes the local site coordination to lower from 9 for *M*1 and 7 for *M*2 to 6. In the position *M*1 (*M*1 = Co1) Co can be considered as bonded to only the six closest O atoms (three symmetry-equivalents of O1 and O2), adopting a metaprismatic coordination, and in *M*2 (*M*2 = Co2) to four symmetry equivalents of O3, O2 and O4 (hydroxyl), forming a distorted octahedron. The sum of six-coordinated Co^{2+} + O^{2-} ionic radii is 2.145 Å (Shannon, 1976) and the

Table 3
Refined atomic positions and occupancy factors for $Ca_{10-x}Co_x(PO_4)_6(OH)_2$, $x = 0$, 0.5, 1.0, 1.5 and 2.0.

Occ = occupancy. For HAp: R_F = 3.86, R_B = 4.83; Co5HAp: R_F = 3.00, R_B = 4.23; Co10HAp: R_F = 2.52, R_B = 4.32; Co15HAp: R_F = 2.62, R_B = 3.29; Co20HAp: R_F = 2.70, R_B = 3.64.

	*M*1	*M*2	P	O1	O2	O3	O4
HAp							
x	1/3	0.2454 (3)	0.3981 (1)	0.3273 (7)	0.5861 (1)	0.3414 (5)	0
y	2/3	0.9936 (3)	0.3696 (1)	0.4850 (6)	0.4648 (7)	0.2559 (4)	0
z	0.0014 (5)	1/4	1/4	1/4	1/4	0.0725 (4)	0.187 (2)
Occ	1/3	1/2	1/2	1/2	1/2	1	0.1666
Co5HAp							
x	1/3	0.2450 (6)	0.3967 (1)	0.329 (1)	0.5848 (2)	0.3441 (9)	0
y	2/3	0.9934 (7)	0.3697 (2)	0.488 (1)	0.464 (1)	0.2602 (8)	0
z	0.002 (1)	1/4	1/4	1/4	1/4	0.0685 (7)	0.178 (3)
Occ (Ca)	0.332 (3)	0.479 (6)	1/2	1/2	1/2	1	0.1666
Occ (Co)	0.001 (3)	0.021 (6)					
Co10HAp							
x	1/3	0.2467 (5)	0.3961 (1)	0.331 (1)	0.5844 (2)	0.3446 (8)	0
y	2/3	0.9960 (7)	0.3675 (2)	0.488 (1)	0.465 (1)	0.2577 (7)	0
z	0.003 (1)	1/4	1/4	1/4	1/4	0.0682 (6)	0.183 (3)
Occ (Ca)	0.317 (3)	0.455 (6)	1/2	1/2	1/2	1	0.1666
Occ (Co)	0.016 (3)	0.045 (6)					
Co15HAp							
x	1/3	0.2475 (5)	0.3959 (1)	0.3349 (1)	0.5841 (2)	0.3457 (1)	0
y	2/3	0.9983 (7)	0.3678 (1)	0.491 (1)	0.467 (1)	0.2558 (8)	0
z	0.005 (1)	1/4	1/4	1/4	1/4	0.0702 (7)	0.179 (3)
Occ (Ca)	0.315 (3)	0.456 (6)	1/2	1/2	1/2	1	0.1666
Occ (Co)	0.018 (3)	0.044 (6)					
Co20HAp							
x	1/3	0.2467 (5)	0.3963 (1)	0.333 (1)	0.5846 (2)	0.3434 (1)	0
y	2/3	0.9977 (5)	0.3678 (1)	0.489 (1)	0.466 (1)	0.2577 (7)	0
z	0.003 (1)	1/4	1/4	1/4	1/4	0.0682 (6)	0.175 (3)
Occ (Ca)	0.324 (3)	0.441 (6)	1/2	1/2	1/2	1	0.1666
Occ (Co)	0.009 (3)	0.059 (6)					

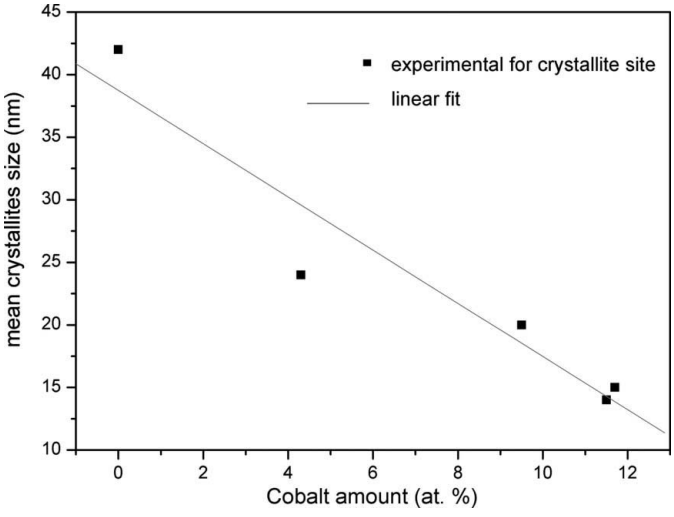

Figure 4
Mean crystallite size of the CoHAp samples as a function of cobalt content.

Table 4
Interatomic distances (Å) in $Ca_{10-x}Co_x(PO_4)_6(OH)_2$, x = 0, 0.5, 1.0, 1.5 and 2.0.

	HAp	Co5HAp	Co10HAp	Co15HAp	Co20HAp
*M*1—O1	2.400 (5) × 3	2.378 (9) × 3	2.380 (9) × 3	2.358 (9) × 3	2.372 (8) × 3
*M*1—O2	2.458 (4) × 3	2.459 (8) × 3	2.467 (7) × 3	2.490 (6) × 3	2.470 (8) × 3
*M*1—O3	2.819 (5) × 3	2.801 (8) × 3	2.786 (7) × 3	2.777 (8) × 3	2.798 (6) × 3
⟨*M*1—O⟩	2.559	2.546	2.544	2.542	2.546
*M*2—O1	2.706 (6)	2.73 (1)	2.75 (1)	2.81 (1)	2.79 (1)
*M*2—O2	2.370 (3)	2.382 (5)	2.356 (5)	2.339 (5)	2.352 (5)
*M*2—O3	2.486 (4) × 2	2.528 (9) × 2	2.488 (8) × 2	2.449 (8) × 2	2.476 (8) × 2
*M*2—O3	2.358 (3) × 2	2.332 (6) × 2	2.335 (5) × 2	2.360 (6) × 2	2.333 (6) × 2
*M*2—O4	2.383 (4)	2.391 (8)	2.384 (7)	2.387 (7)	2.387 (7)
⟨*M*2—O⟩	2.450	2.460	2.448	2.450	2.449
P—O1	1.534 (7)	1.53 (1)	1.53 (1)	1.53 (1)	1.53 (1)
P—O2	1.534 (1)	1.534 (2)	1.534 (2)	1.53 (2)	1.534 (2)
P—O3	1.533 (3) × 2	1.533 (6) × 2	1.534 (5) × 2	1.533 (6) × 2	1.533 (5) × 2
⟨P—O⟩	1.533	1.533	1.533	1.532	1.532

observed average Ca1/Co1—O and Ca2/Co2—O bond distances for CN = 6 are in the intervals 2.430–2.422 and 2.407–2.393 Å, respectively.

Decreasing average M—O distances as a consequence of the insertion of smaller ions in the HAp structure causes deviations from regular anion nets. These phenomena can be described based on the variation of the twist angle φ (O1—M1—O2) of the $M1O_6$ metaprism. White & ZhiLi (2003) have shown that φ increases linearly with a decrease in crystal radii and unit-cell volume. The twist angle φ (O1—M1—O2) of the $M1O_6$ metaprism changed from 23.81 to 23.57, 23.38, 22.31 and 22.35° for HAp, Co5HAp, Co10HAp, Co15HAp and Co20HAp, respectively. The small amount of Co content in the apatite structure (HAp, Co5HAp and Co10HAp) causes an insignificant transition of the φ angle. Furthermore, it was observed (Henderson *et al.*, 2009) that Ca in the M1 position is too small for an $M1O_6$ polyhedron so that the twist angles are smaller than expected. We suppose that a smaller cation such as cobalt provokes a similar phenomenon.

The P—O bond distances are within the expected ranges found in other phosphates (Table 4), with average bond lengths of 1.533, 1.533, 1.533, 1.532 and 1.532 for HAp, Co5HAp, Co10HAp, Co15HAp and Co20HAp, respectively.

The cobalt content in the CoHAp powders calculated from the refined occupations of the atomic sites is 0, 2.6, 7.3, 7.4 and 8.1 at.% for HAp, Co5HAp, Co10HAp, Co15HAp and Co20HAp, respectively. Bearing in mind that the cobalt amount is small and that the powders have low crystallinity, and also that the occupancy cannot be satisfactorily extracted, these results show good enough agreement with the data obtained by chemical analysis (0, 4.3, 9.5, 11.7 and 11.5 at.%, respectively).

The changes in the crystallite size and morphology with increasing amount of cobalt in CoHAp were additionally confirmed by TEM and HRTEM analyses. TEM images of the pure HAp and Co15HAp powders are presented in Figs. 6(*a*) and 6(*b*), respectively. The morphology of the samples is affected by the presence of cobalt in the structure. Pure HAp (Fig. 6*a*) is constituted of randomly oriented, elongated rods of similar sizes, which is in accordance with the Rietveld refinement results. The Co15HAp sample with the highest degree of substitution shows significantly reduced elongation (Fig. 6*b*). This powder consists of randomly oriented flake-like particles. HRTEM images provide further insight into the morphology and structural details of the studied hydro-

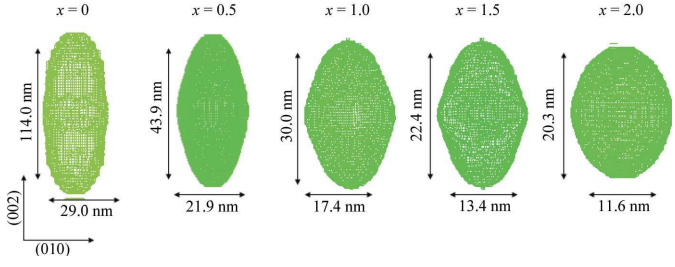

Figure 5
Representation of the change in morphology and crystallite size with increasing cobalt amount in $Ca_{10-x}Co_x(PO_4)_6(OH)_2$.

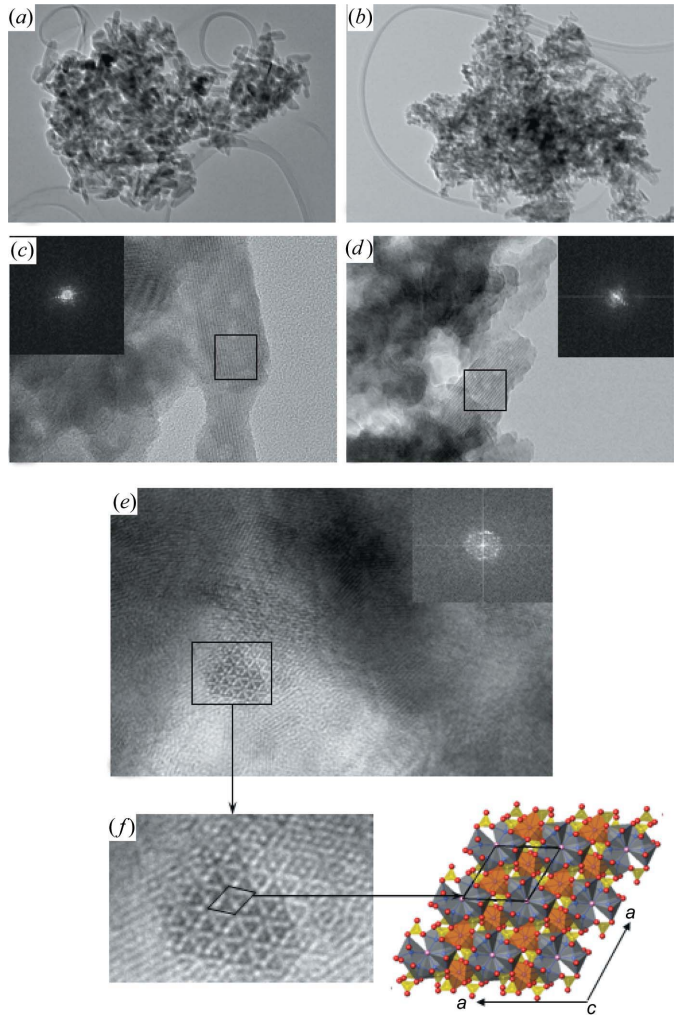

Figure 6
TEM images of HAp (*a*) and Co15HAp (*b*), HRTEM images of HAp (*c*) and Co15HAp (*d*), (*e*), (*f*).

xyapatites. The HRTEM morphology and the corresponding fast Fourier transform (FFT) confirmed the hexagonal symmetry of the two analysed powders HAp (Fig. 6*c*) and Co15HAp (Fig. 6*d*).

The data for HAp (Fig. 6*c*) show two sets of lattice fringes corresponding to the lattice planes (200) and (300), with lattice spacing *d* of 4.1 and 2.7 Å, respectively, which corresponds to the literature data for HAp with the same chemical composition (Table 1). The calculated FFT of Co15HAp powder shows four sets of crystallographic planes (inset of Fig. 6*d*). Three of these cut the crystallographic *a* axis and correspond to (100), (200) and (300) planes with related *d* values of 8.0, 4.0 and 2.7 Å, respectively, which are close to 8.2, 4.1 and 2.7 Å, obtained for pure HAp. The fourth calculated set of lattice fringes for (002) planes displays a *d* value of 3.4 Å. Fig. 6(*e*) shows the HRTEM image and the calculated FFT (inset) of the crystallite oriented perpendicular to the *c* axis of Co15HAp crystals. The data show two sets of crystallographic planes (300) and (210) with related *d* values of 2.7 and 2.9 Å, respectively. Fig. 6(*f*) shows the image of the HAp structure presented perpendicularly on the crystallographic *c* axis.

4. Conclusion

A new series of cobalt-substituted calcium hydroxyapatite $[Ca_{10-x}Co_x(PO_4)_6(OH)_2]$ ($x \simeq 0.00$–0.12) nanopowders were synthesized by hydrothermal treatment of a precipitate. The results of ICP analysis and Rietveld analysis showed that, under the given conditions of hydrothermal processing, the maximal amount of incorporated cobalt ions in HAp was saturated at approximately 12 at.%; further increase in the cobalt reagent concentration did not increase the amount of Co^{2+} in the investigated crystal structure. The values of the unit-cell parameters and cell volume gradually decreased with the increase in cobalt content in the structure, which explicitly indicates the replacement of Ca^{2+} by smaller Co^{2+}. The incorporation of cobalt ions in the calcium crystallographic positions was confirmed by vibrational spectroscopy; in addition, the 2+ oxidation state of cobalt ions in the CoHAp samples was confirmed by magnetic measurements.

Microstructural analysis showed a significant decrease in the average crystallite size, from 40 to 26 nm, with incorporation of 4.3 at.% of cobalt ions in both crystallographic positions of calcium. The increase in cobalt content to ~12 at.% slightly reduced the average crystallite size down to 14 nm. The results of the Rietveld refinement (unit-cell parameters, the shape and size of the crystallites) are in good agreement with the results of TEM and HRTEM analyses.

The Ministry of Science and Technological Development of the Republic of Serbia provided financial support under grant No. 142006. The authors are grateful to Dr Lidija Mančić, Dr Milovan Stoiljković, Dr Vladan Kusigerski and Dr Miodrag Mitrić for their kind help in the analysis of structural and TEM results, as well as the chemical analysis.

References

Anmin, H., Ming, L., Chengkang, C. & Dali, M. (2007). *J. Mol. Catal. A Chem.* **267**, 79–85.
Antić, B., Kremenović, A., Nikolić, A. S. & Stoiljković, M. (2004). *J. Phys. Chem. B*, **108**, 12646–12651.
Badraoui, B., Aissa, A. & Debbabi, M. (2007). *J. Phys. Chem. Solids*, **68**, 211–216.
Badraoui, B., Bigi, A., Debbabi, M., Gazzano, M., Norberto, R. & Thouvenot, R. (2001). *Eur. J. Inorg. Chem.* **2001**, 1261–1267.
Baikie, T., Ng, G. M. H., Madhavi, S., Pramana, S. S., Blake, K., Elcombe, M. & White, T. J. (2009). *Dalton Trans.* pp. 6722–6726.
Bigi, A., Ripamonti, A., Brückner, S., Gazzano, M., Roveri, N. & Thomas, S. A. (1989). *Acta Cryst.* B**45**, 247–251.
Brückner, S., Lusvardi, G., Menabue, L. & Saladini, M. (1995). *Inorg. Chim. Acta*, **236**, 209–212.
Cvejic, Z., Rakic, S., Kremenovic, A., Antic, B., Jovalekic, C. & Colomban, P. (2006). *Solid State Sci.* **8**, 908–915.
De Leeuw, N. H. (2001). *Chem. Commun.* pp. 1646–1647.
Denton, A. R. & Ashcroft, N. W. (1990). *Phys. Rev. A*, **43**, 3161–3664.
Dodd, S. J., Williams, M., Suhan, J. P., Williams, D. S., Koretsky, A. P. & Ho, Ch. (1999). *Biophys. J.* **76**, 103–109.
Đordević, T., Šutović, S., Stojanović, J. & Karanović, Lj. (2008). *Acta Cryst.* C**64**, i82–i86.
Elkabouss, K., Kacimi, M., Ziyad, M., Ammar, S. & Bozon-Verduraz, F. (2004). *J. Catal.* **226**, 16–24.
Elliott, J. C. (1994). *Structure and Chemistry of the Apatites and Other Calcium Orthophosphates.* Amsterdam: Elsevier.
Elliott, J. C., Mackie, P. E. & Young, R. A. (1973). *Science*, **180**, 1055–1057.
Ergun, C. (2008). *J. Eur. Ceram. Soc.* **28**, 2137–2149.
Garvey, R. G. (1986). *Powder Diffr.* **B1**, 114–116.
Henderson, C. M. B., Bell, A. M. T., Charnock, J. M., Knight, K. S., Wendlant, R. F., Plant, D. A. & Harrison, W. J. (2009). *Mineral. Mag.* **73**, 433–455.
Hughes, J. M., Cameron, M. & Crowley, K. D. (1989). *Am. Mineral.* **74**, 870–876.
Jain, T. K., Richey, J., Strand, M., Leslie-Pelecky, D. L., Flask, C. A. & Labhasetwa, V. (2008). *Biomaterials*, **29**, 4012–4021.
Järvinen, M. (1993). *J. Appl. Cryst.* **26**, 525–531.
Jeanjean, J., Vincent, U. & Fedoroff, M. (1994). *J. Solid State Chem.* **108**, 68–72.
Jevtić, M., Mitrić, M., Škapin, S., Jančar, B., Ignjatović, N. & Uskoković, D. (2008). *Cryst. Growth Des.* **8**, 2217–2222.
Kannan, S., Goetz-Neunhoeffer, F., Neubauer, J. & Ferreria, M. F. (2008). *J. Am. Ceram. Soc.* **91**, 1–12.
Kay, M. I., Young, R. A. & Posner, A. S. (1964). *Nature* (*London*), **204**, 1050−1052.
Kazin, P. E., Gazizova, O. R., Karpov, A. S., Jansen, M. & Tretyakov, Y. D. (2007). *Solid State Sci.* **9**, 82–87.
Kuo, Y.-K., Liou, B.-T., Yen, S.-H. & Chu, H.-Y. (2004). *Opt. Commun.* **237**, 363–369.
Li, M., Xiao, X., Liu, R., Chen, C. & Huang, L. (2008). *J. Mater. Sci. Mater. Med.* **19**, 797–803.
Low, H. R., Phonthammachai, N., Maignan, A., Stewart, G. A., Bastow, T. J., Ma, L. L. & White, T. J. (2008). *Inorg. Chem.* **47**, 11774–11782.
Ma, X. & Ellis, D. E. (2008). *Biomaterials*, **29**, 257–265.
McCusker, L. B., Von Dreele, R. B., Cox, D. E., Louër, D. & Scardi, P. (1999). *J. Appl. Cryst.* **32**, 36–50.
Mostafa, N. Y. & Brown, P. W. (2007). *J. Phys. Chem. Solids*, **68**, 431–437.
Pan, H.-B. & Darvell, B. W. (2009). *Cryst. Growth Des.* **9**, 639–645.
Pankhurst, Q. A., Connolly, J., Jones, S. K. & Dobson, J. (2003). *J. Phys. D Appl. Phys.* **36**, 167–181.
Pearson, R. G. (1988). *Inorg. Chem.* **27**, 734–740.
Posner, A. S., Perloff, A. & Diorio, A. F. (1958). *Acta Cryst.* **11**, 308–309.

Riberio, C. C., Gibson, I. & Barbosa, M. A. (2006). *Biomaterials*, **27**, 1749–1761.
Rodrigez-Carvajal, J. (1990). *FULLPROF: a Program for Rietveld Refinement and Pattern Matching Analysis.* Abstracts of the Satellite Meeting on Powder Diffraction of the XV Congress of the IUCr, Toulouse, France, p. 127.
Rodriguez-Carvajal, J. (2005). *FullProf2k*. Version 2.40-May 2005-LLB JRC. Laboratoire Léon Brillouin (CEA–CNRS), CEA–Sarclay, France.
Rodriguez-Lorenzo, L. M., Hart, J. N. & Gross, K. A. (2003). *J. Phys. Chem. B*, **107**, 8316–8320.
Roisnel, T. & Rodrigez-Carvajal, J. (2001). *Mater. Sci. Forum*, **378–391**, 118–123.
Shannon, R. D. (1976). *Acta Cryst.* A**32**, 751–767.
Shi, P., Geng, F. & Cheng, F. T. (2006). *Mater. Lett.* **60**, 1996–1999.
Stephens, P. W. (1999). *J. Appl. Cryst.* **32**, 281–289.
Stojanović, Z., Veselinović, Lj., Marković, S., Ignjatović, N. & Uskoković, D. (2009). *Mater. Manuf. Processes*, **24**, 1096–1103.
Stork, L., Mueller, P., Dronskowski, R. & Ortlepp, J. R. (2005). *Z. Kristallogr.* **220**, 201–205.
Sudarsanan, K. & Young, R. A. (1969). *Acta Cryst.* B**25**, 1534–1543.
Suetsugu, Y. & Tanaka, J. (2002). *J. Mater. Sci. Mater. Med.* **13**, 767–772.
Suvorova, E. I. & Buffat, P. A. (2001). *Eur. Cell Mater.* **1**, 27–42.
Vallet-Regi, M. & Arcos, D. (2005). *J. Mater. Chem.* **15**, 1509–1516.
Wang, J., Nonami, T. & Yubata, K. (2008). *J. Mater. Sci: Mater. Med.* **19**, 2663–2667.
White, T. J. & ZhiLi, D. (2003). *Acta Cryst.* B**59**, 1–16.
Wu, H.-Ch., Wang, T.-W., Sun, J.-Sh., Wang, W.-H. & Lin, F.-H. (2007). *Nanotechnology*, **18**, 165601.
Young, R. A. (1993). *Rietveld Refinement.* Oxford University Press.
Yuanzhi, T., Helen, F. C., Martin, T. D., Richard, J. R. & Young, J. L. (2009). *Biomaterials*, **30**, 2864–2872.
Zhu, K., Yanagisawa, K., Shimanouchi, R., Onda, A. & Kajiyoshi, K. (2006). *J. Eur. Ceram. Soc.* **26**, 509–513.